

Investigation of the flow field in thin polymer films due to inhomogeneous drying

Philipp Cavadini, Joachim Erz, Dirk Sachsenheimer, Anne Kowalczyk,
Norbert Willenbacher, Philip Scharfer, Wilhelm Schabel

© American Coatings Association 2015

Abstract In the field of organic and printed electronics (e.g., polymer solar cells, OLEDs, or Li-ion batteries), there is a growing demand for thin functional layers with highly homogeneous surface topology. If these layers are coated from the liquid phase, the coating and drying steps affect the surface quality. As a result of inhomogeneous drying rates, the solvent concentration can vary along the top surface and the thickness of a solidifying solution, leading to local differences in surface tension. In turn, Marangoni convection, as the balancing mechanism, can occur and cause surface inhomogeneity. The in situ reconstruction of the free surface during drying has been presented elsewhere. During this investigation phenomena occurred that could not be completely understood without knowledge of the respective flow field. In the present work, the visualization of the flow field in thin polymer films [methanol-poly(vinyl acetate) solution with 67 wt% methanol] due to inhomogeneous drying is presented. To resolve the flow field, we apply fluorescent particle tracking (μ PTV). Since both measurement techniques cannot easily be applied at the same time, the boundary conditions were adapted to the way of observation of each experimental setup. In

the case of the setup for surface reconstruction of the free surface, locally different evaporation rates were realized by drying on a structured substrate (varying material). To force similar variation of the drying conditions in the case of the μ PTV setup, the drying film was partially covered. As expected, both boundary conditions result in a propagating wave front towards regions of high surface tension. Combining both experimental setups, we were able to visualize the free surface and the flow structures up- and downstream of the wave front and found different flow regimes.

Keywords Measurement and instrumentation, μ PTV, Marangoni convection, Surface deformation, Flow visualization

Introduction

In many thin film applications such as organic and printed electronics, biosensors and optical coatings, there is a growing demand for functional layers with highly homogeneous surface topology.^{1–3} A deviation in layer thickness will result in lateral performance variations (e.g., intensity of an OLED³). The surface tension of the applied polymer–solvent solutions is a function of the solvent content and the temperature (see Fig. 1, left). Since both parameters (temperature and concentration) alter as drying proceeds, inhomogeneous evaporation rates lead to gradients in surface tension.

Depending on the direction and evolution of the occurring gradients, shear stresses at the surface occur. The stress at the surface is transferred into surface flow and due to viscosity a flow in the bulk fluid arises (Marangoni–Bénard convection) that potentially leads to a deformation of the free surface.^{5,6} In addition, fluid flow from regions of low evaporation to regions of relatively higher evaporation may occur as has been shown by reference (7). Inhomogeneous evaporation

This paper was presented at the 17th International Coating Science and Technology Symposium, September 7–10, 2014, in San Diego, CA (USA).

P. Cavadini (✉), J. Erz, P. Scharfer,
W. Schabel

Thin Film Technology, Institute of Thermal Process
Engineering, Karlsruhe Institute of Technology,
Karlsruhe 76131, Germany
e-mail: philipp.cavadini@kit.edu

D. Sachsenheimer, A. Kowalczyk, N. Willenbacher
Applied Mechanics, Institute of Mechanical Process
Engineering, Karlsruhe Institute of Technology,
Karlsruhe 76131, Germany

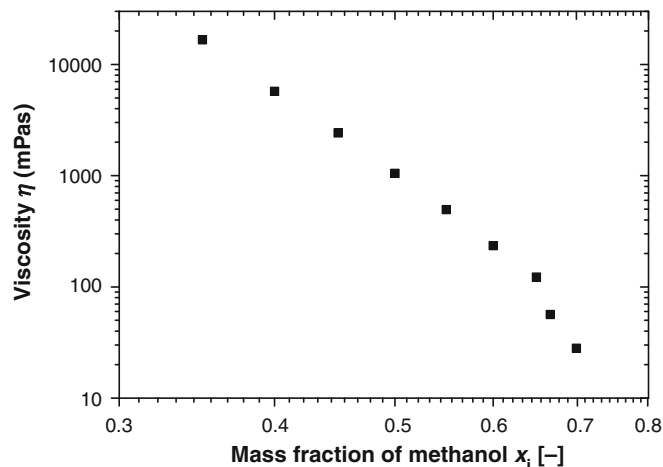
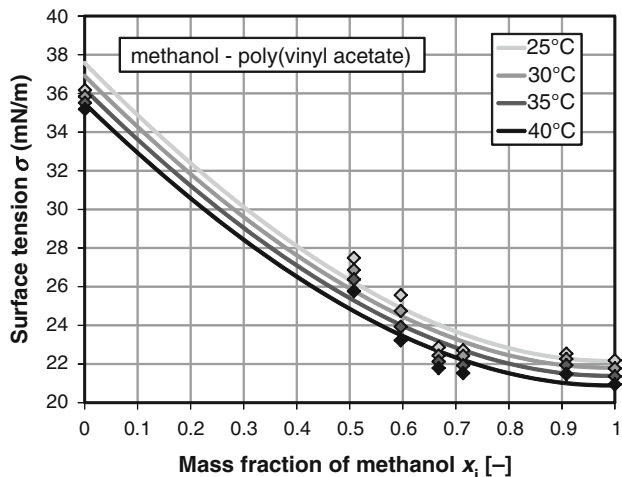


Fig. 1: Surface tension σ of a binary methanol-poly(vinyl acetate) (molecular weight PVAc, $M_W = 55,000 - 70,000 \text{ g/mol}$) solution as a function of solvent content and temperature (left,⁴) and viscosity of a binary methanol-poly(vinyl acetate) solution as a function of solvent content (right)

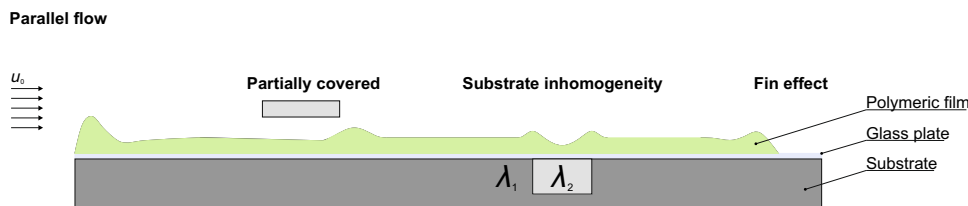


Fig. 2: Possible reasons (boundary conditions) for surface deformation due to surface tension-driven flows⁴

rates may appear as a result of local differences in the flow conditions of the surrounding drying gas, by varying material properties of the substrate or the fin effect (see Fig. 2). Since in industrial application the relevant parameters are various (e.g., inhomogeneous drying conditions, multicomponent systems), a profound understanding of the driving forces for Marangoni convection and the appearing surface deformation are needed.

To gain further understanding of the surface deformations of polymer solutions occurring as a result of inhomogeneous drying conditions, two measurement systems are utilized. Earlier we presented the in situ reconstruction of the free surface of a thin transparent polymer solution drying on a structured substrate.⁴ Since certain observations could not finally be understood by solely resolving the surface topology over time, we now use a μ PTV-system⁸ to resolve the flow field in the film. Both systems are based on optics but resulting from the different ways of observation of each measurement setup, it is not possible to apply both systems simultaneously. Hence, boundary conditions adapted to each system, expected to deliver comparable results and allowing connection of the findings, have been chosen. Both boundary conditions have been set to force a gradient in the distribution of the drying rate. In the case of the measurement system

to reconstruct the surface topology, the optical system observes from above. Here we use a patterned surface (varying material) resulting in a local dependency of the heat transfer rate into the film and therefore in a local dependency of the drying rate. The μ PTV-system is based on an inverse fluorescent microscope. Here, we partially cover the drying film to induce a local dependency of the drying rate. In both cases, we observe mass transport to regions of high surface tension resulting in a surface wave remaining in the dried film. Furthermore, using the surface reconstruction setup, we visualized small surface humps whose appearance showed a dependency on location.⁴ Analyzing the flow structure, we found these humps to be a result of short-range convection cells. The local dependency has been assumed to be a result of the superposition of the flow causing the wave front and short-range fluctuations.

Measurement system

In order to visualize the flow field throughout the film, 1.5- μm green fluorescent polystyrene microspheres (solid: 1%, i.d. 0.52 μm , (Bangs Laboratories, Inc.TM)) were added to 75 μl polymer solution. A scheme of the

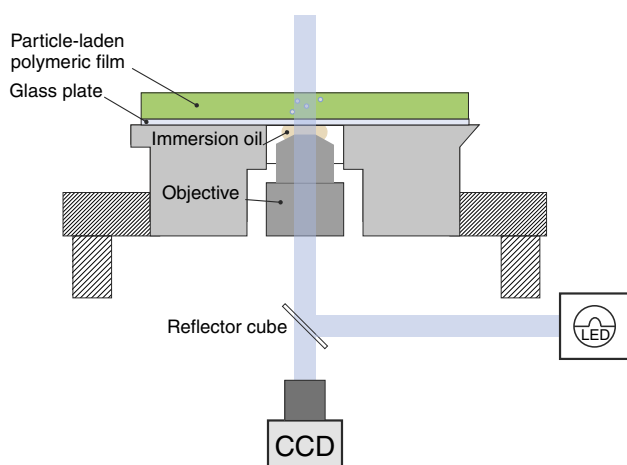


Fig. 3: Test rig for flow field visualization using fluorescent particle tracking. The system consists of an inverted fluorescence microscope equipped with an immersion lens, a CCD camera to capture images, and an LED light source

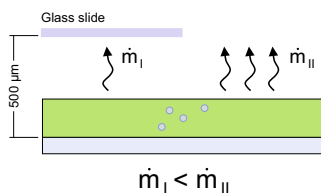


Fig. 4: Schematic drawing of the boundary condition applied in the case of the flow field visualization experiments. The drying film ($h_0 \sim 150 \mu\text{m}$) is partially covered by a glass slide ($h_0 \sim 500 \mu\text{m}$)

test rig is displayed in Fig. 3. To observe the particle movement, an inverted fluorescence microscope (Zeiss Observer D1) equipped with a $100\times$ oil immersion lens (N.A. 1.3) is connected to a CCD camera. The used light source is a Colibri-LED (470 nm) from Zeiss. Images are captured using a digital AVT Pike F100B CCD camera. To address the focus plane of the optical system and to perform depth-scans, an automatic z-scan is integrated into the system. The step size and the starting position are adjusted to the shrinkage of the film. The starting position is determined by the location of the free surface which can be tracked in a parallel process by grayscale analysis. All drying experiments are conducted at laboratory temperature ($T_L = 20^\circ\text{C}$).

Since we use an inverse fluorescence microscope to track the tracer particles, a structured substrate has no option to induce a local dependency of the drying rate. Here, we use a glass slide placed $500 \mu\text{m}$ above the substrate, allowing it to partially cover the cast film ($h_0 \sim 150 \mu\text{m}$). Hence, the cast film can be distinguished in a region with hindered mass transfer and a region with ambient conditions (see Fig. 4).

The evaluation process is based on routines implemented in MATLAB[®] for grayscale analysis which

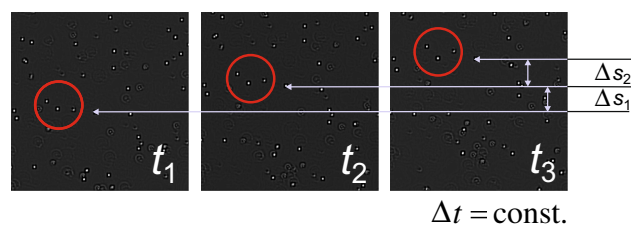


Fig. 5: Principle of the velocity evaluation from a set of pictures using fluorescent particle tracking. The velocities can be evaluated using the Störmer–Verlet algorithm. The time step between two images is constant

track the center of gravity of each particle in every captured frame and connect the respective locations to particle trajectories. Using a Störmer–Verlet-like method,⁹ the particle trajectories are translated into the respective velocities. To decrease a potential error on the determined velocity distribution arising from, e.g., Brownian motion,¹⁰ we average over 40 images (fps = 20) to get the velocity at a certain location and time. Figure 5 exemplarily shows a series of three pictures taken at a constant distance to the substrate within a horizontally directed flow field. Running the automatic z-scan in a loop, the 3D velocity profile of a horizontal flow can be resolved layer by layer over film height and drying time.

In the case of 3D flow structures we use the approach of deconvolution microscopy.⁸ To resolve the line-of-sight velocity component, the size of the point spread function (PSF) appearing as a result of optical diffraction is correlated to the distance of a particle to the focus plane. Hence, a volumetric analysis of the flow field (3D-3C) becomes possible. The accessible depth-of-field in the line-of-sight direction depends on the used lens.¹¹ Figure 6 shows particles at different distances to the focus plane (left) and a rendering of a depth-scan visualizing the PSF performed in a dried film (right).

Frissen Gibson and Lanni¹² present a theoretical approach to predict the PSF. In a first attempt, experimental data are used to correlate the diameter of the diffraction ring pattern and the distance to the focus plane.^{13–15} Figure 7 shows the calibration for the used system based on a series of five pictures of immobilized particles in a dry film. Moving the particle off focus in steps of $1 \mu\text{m}$, a characteristic for the used system (camera and lens) can be generated. Hence, the optical setup allows tracking particles for the range of $\sim 4 \mu\text{m}$ in the line-of-sight direction.

Results and discussion

Since the field of view of the macroscopic optic used for the surface reconstruction experiments⁴ and the field of view of the microscopic optic used for the flow field visualization differ by orders of magnitude, we

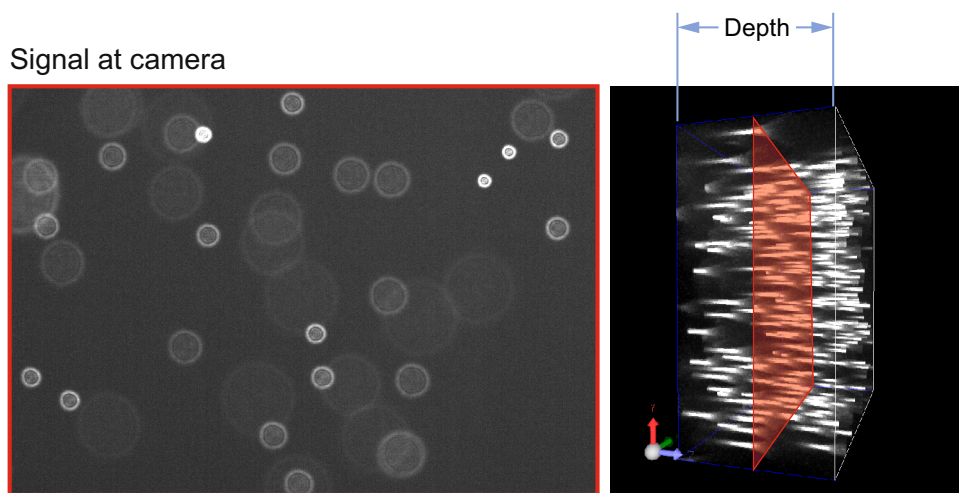


Fig. 6: Unprocessed image taken during a drying experiment showing particles at different distances to the focus plane (left) and rendered depth-scan showing PSF in a dried film (right)

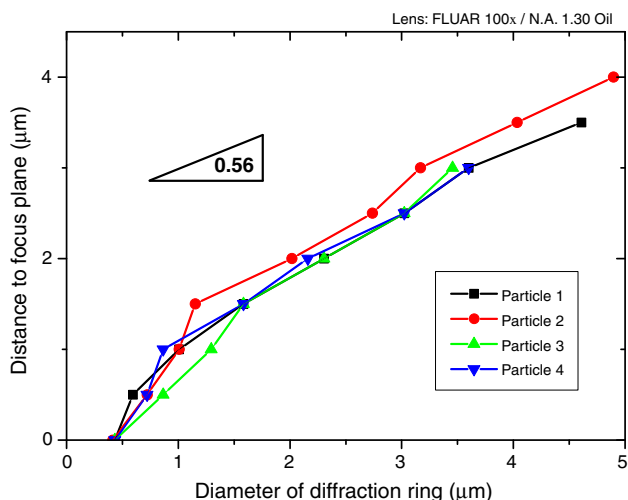


Fig. 7: Calibration of the 100× oil immersion objective for a polystyrene particle ($d = 0.5 \mu\text{m}$) in PVAc

chose three measurement positions that represent the different flow regimes: (1) center of the covered area, (2) transition region, and (3) uncovered area (see Fig. 8 scheme).

First the observations made for the flow field occurring in the covered region will be discussed. The measuring position is located $\sim 5 \text{ mm}$ away from the edge centered in the covered region. The respective velocity profiles over film height obtained by depth-scans are shown in Fig. 9. After an onset of around $\sim 60 \text{ s}$ a unidirectional flow field towards the uncovered area develops. The gradient in surface tension causes a surface flow and the lower fluid layers are dragged along. With increasing drying time, the film shrinks and viscosity increases. The increasing viscosity damps the driving forces until finally the entire fluid motion freezes.

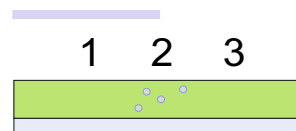


Fig. 8: Scheme of the regions of interest: Center of the covered region (1), transition region (2), and uncovered region (3)

Flow profiles of the region between the covered and the uncovered area (for location see Fig. 8 (position 2)) are shown in Fig. 10. The onset time of unidirectional fluid motion is less in this area, and the particle velocities are much larger than in the covered region with a maximum measured velocity of $v_{\text{max}} = 98 \pm 12 \mu\text{m/s}$. After an initial acceleration and the development of a nearly linear flow profile, a flattening of the velocity profiles begins (triangular symbols in Fig. 10). This is supposed to be a result of the solvent concentration profile over the film height developing during drying.¹⁶ Hence, the layers closer to the surface are of lower solvent concentration and therefore of higher viscosity (Fig. 1, right). Due to the increasing viscosity, the velocity decreases further until the film is dry. The increase in film height in the period between $t = 190 \text{ s}$ (4) and $t = 212 \text{ s}$ (5) indicates the accumulation of mass in the transition region as a result of the directed flow field.

Third, we analyze the flow field in the uncovered area ($\sim 5 \text{ mm}$ away from the cover). Here, a horizontal unidirectional flow field was not observed. Instead the region was dominated by microscale 3D convection cells in the range of $\sim 40 \mu\text{m}$. Figure 11 exemplarily shows the visualization by particle trajectories of a convection cell. Within the center of the convection cell, the particles rise up to the surface from where they

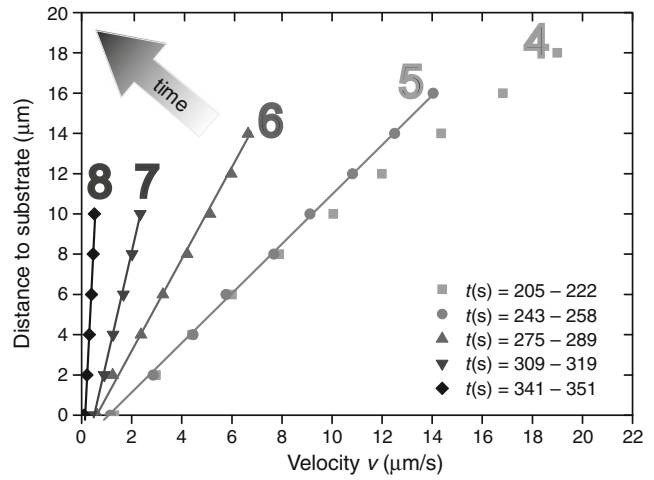
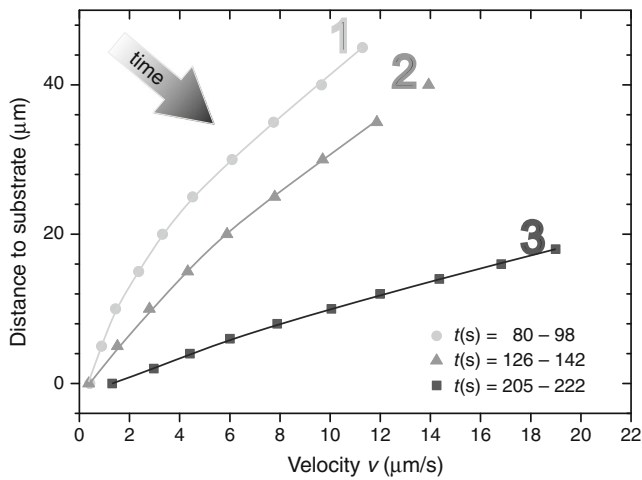


Fig. 9: Velocity profiles (at the center of the covered area Fig. 8, (1)) over film height at different drying times. At the beginning of drying (left), velocity profiles No. 1–3 and until the end of drying (right), velocity profiles No. 4–8. Methanol-poly(vinyl acetate) solution with 67 wt% methanol: $T_{\infty} = 20^{\circ}\text{C}$ and $s_0 \approx 150 \mu\text{m}$. The inhomogeneous drying conditions are applied by partially covering the film

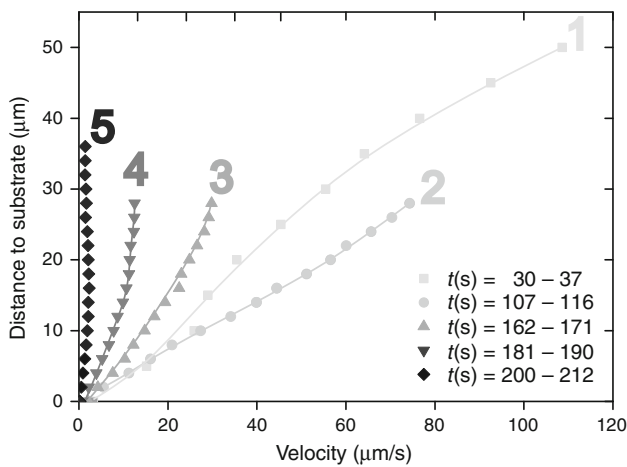


Fig. 10: Velocity profiles at the transition area (Fig. 8, (2)). Methanol-poly(vinyl acetate) solution with 67 wt% methanol: $T_{\infty} = 20^{\circ}\text{C}$ and $s_0 \approx 150 \mu\text{m}$. The inhomogeneous drying conditions are applied by partially covering the film

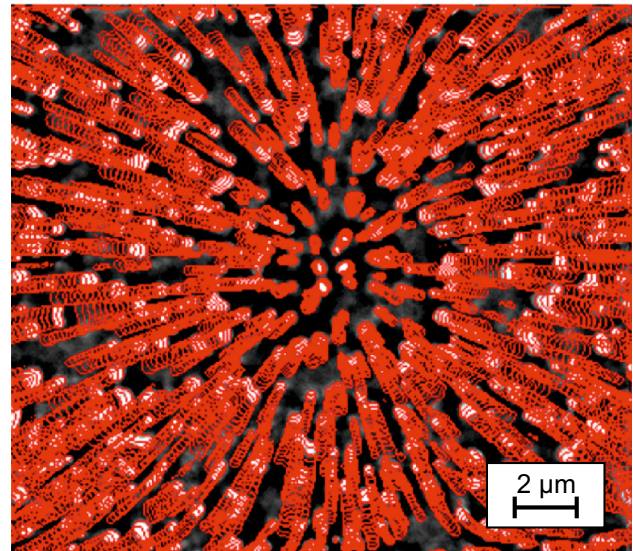


Fig. 11: Center of a stationary convection cell visualized by particle trajectories. Within the center of the convection cell, the particles rise up to the surface from where they spread radially

radially spread outwards. This flow structure explains the humped surface topology visualized upstream of the wave front using the surface reconstruction setup. Comparing the different flow fields up- and downstream of the propagating wave front, the local dependency of the occurring surface humps becomes understandable. Since the convection cells appear as a result of microscale fluctuations of the temperature at the free surface inducing bulk fluid motion, the presence of the unidirectional flow field suppresses their appearance.

As a final step, cross profile measurements (Dektak M6, Veeco) of the dried films resulting from the two boundary conditions have been performed (see Fig. 12). As expected, the directed mass transport and the resulting surface wave can be found in the dry film. Although the curves do not match, the basic features can be found in both cases. The main difference appears in the range from which material has been attracted.

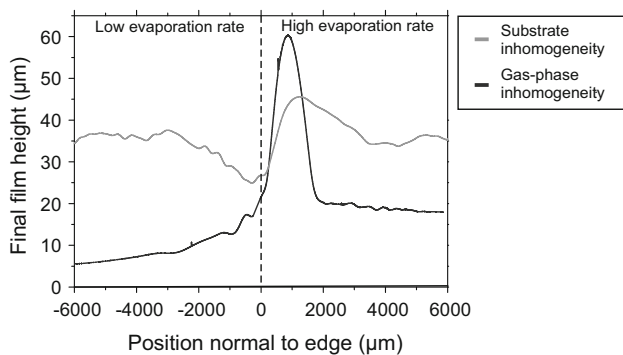


Fig. 12: Cross profiles of the dried film normal to the cover. Methanol-poly(vinyl acetate) solution with 67 wt% methanol. Black: Drying conditions: Film partially covered, $T_\infty = 20^\circ\text{C}$ and $s_0 \approx 150 \mu\text{m}$. Gray: Drying conditions: Channel flow over patterned substrate, $u_\infty = 0.5\text{m/s}$, $T_\infty = 25^\circ\text{C}$ and $s_0 \approx 150 \mu\text{m}$

Conclusions

In the present work, we present the visualization of the flow field occurring in binary polymer solution [methanol-poly(vinyl acetate) with 67 wt% methanol] by partially covering while drying. Earlier we presented the investigation of the surface deformation as a result of inhomogeneous drying conditions.⁴ Since both measurement setups differ essentially in the way of observation and therefore could not be used at the same time, a pair of boundary conditions has been defined that allowed comparability of the findings. In both cases, the boundary conditions were set to create two neighboring rectangular regions with different evaporation rates. In the case of the surface reconstruction, we observe from the top of the drying film and therefore create inhomogeneous drying by casting on a patterned surface. In the case of the flow field visualization, we partly cover the film to achieve a local dependency of the evaporation rate. In both cases, we visualized the material transport towards regions of relatively high surface tension. We could distinguish different flow regimes depending on location and use the findings regarding the flow field to explain the different surface topologies occurring during drying.

References

1. Moule, AJ, Bonekamp, JB, Meerholz, K, "The Effect of Active Layer Thickness and Composition on the Performance of Bulk-Heterojunction Solar Cells." *J. Appl. Phys.*, **100** (9) 094503 (2006)
2. Kirchartz, T, et al., "Understanding the Thickness-Dependent Performance of Organic Bulk Heterojunction Solar Cells: The Influence of Mobility, Lifetime, and Space Charge." *J. Phys. Chem. Lett.*, **3** (23) 3470–3475 (2012)
3. Vieyra Salas, JA, et al., "Active Control of Evaporative Solution Deposition by Modulated Infrared Illumination." *J. Phys. Chem C*, **116** (22) 12038–12047 (2012)
4. Cavadini, P, et al., "Investigation of Surface Deformation During Drying of Thin Polymer Films Due to Marangoni Convection." *Chem. Eng. Process. Process. Intensif.*, **64** 24–30 (2013)
5. Levich, VG, Krylov, VS, "Surface Tension Driven Phenomena." *Annu. Rev. Fluid Mech.*, **1** 293–316 (1969)
6. Harris, DJ, Lewis, JA, "Marangoni Effects on Evaporative Lithographic Patterning of Colloidal Films." *Langmuir*, **24** (8) 3681–3685 (2008)
7. Harris, DJ, et al., "Patterning Colloidal Films via Evaporative Lithography." *Phys. Rev. Lett.*, **98** (14) 148301 (2007)
8. Park, JS, Kihm, KD, "Three-Dimensional Micro-PTV Using Deconvolution Microscopy." *Exp. Fluids*, **40** (3) 491–499 (2006)
9. Griebel, M, et al., *Numerische Simulation in der Moleküldynamik: Numerik, Algorithmen, Parallelisierung, Anwendungen*, p. 480. Springer, Berlin (2004)
10. Santiago, JG, et al., "A Particle Image Velocimetry System for Microfluidics." *Exp. Fluids*, **25** (4) 316–319 (1998)
11. Inoué, S, Spring, KR, *Video Microscopy: The Fundamentals*. Plenum Press, New York (1997)
12. Frisken Gibson, S, Lanni, F, "Experimental Test of an Analytical Model of Aberration in an Oil-Immersion Objective Lens Used in Three-Dimensional Light Microscopy." *J. Opt. Soc. Am. A*, **9** (1) 154–166 (1992)
13. Park, JS, Choi, CK, Kihm, KD, "Temperature Measurement for a Nanoparticle Suspension by Detecting the Brownian Motion Using Optical Serial Sectioning Microscopy (OSSM)." *Meas. Sci. Technol.*, **16** (7) 1418 (2005)
14. Speidel, M, Joná, A, Florin, E-L, "Three-Dimensional Tracking of Fluorescent Nanoparticles with Subnanometer Precision by Use of Off-Focus Imaging." *Opt. Lett.*, **28** (2) 69–71 (2003)
15. Wu, M, Roberts, JW, Buckley, M, "Three-Dimensional Fluorescent Particle Tracking at Micron-Scale Using a Single Camera." *Exp. Fluids*, **38** (4) 461–465 (2005)
16. Schabel, W, *Trocknung von Polymerfilmen-Messung von Konzentrationsprofilen mit der Inversen-Mikro-Raman-Spektroskopie*, in *Institut für Thermische Verfahrenstechnik*. Universität Karlsruhe (TH), Karlsruhe (2004)